JACS
JOURNAL OF THE AMERICAN CHEMICAL SOCIETY

ARTICLE

pubs.acs.org/JACS

Pressure-Induced Structural, Magnetic, and Transport Transitions in the Two-Legged Ladder $Sr_3Fe_2O_5$

Takafumi Yamamoto,[†,‡] Cédric Tassel,[†,‡] Yoji Kobayashi,[†] Takateru Kawakami,[§] Taku Okada,[⊥] Takehiko Yagi,[⊥] Hideto Yoshida,[∥] Takanori Kamatani,[∥] Yoshitaka Watanabe,[∥] Takumi Kikegawa,[¶] Mikio Takano,[#] Kazuyoshi Yoshimura,[‡] and Hiroshi Kageyama*[,†,‡,#]

[†]Department of Energy and Hydrocarbon Chemistry, Graduate School of Engineering, Kyoto University, Kyoto 615-8510, Japan

[‡]Department of Chemistry, Graduate School of Science, Kyoto University, Kyoto 606-8412, Japan

[§]Institute of Quantum Science, Nihon University, Chiyoda, Tokyo 101-8308, Japan

[⊥]Research Institute for Solid State Physics, University of Tokyo, 5-1-5 Kashiwanoha, Kashiwa, Chiba 277-8581, Japan

[∥]Graduate School of Science and Technology, Nihon University, Chiyoda-ku, Tokyo 101-8308, Japan

[¶]Photon Factory, Institute of Material Structure Science, High Energy Acceleration Research Organization (KEK), 1-1 Oho, Tsukuba, Ibaraki 305-0801, Japan

[#]Institute for Integrated Cell-Material Sciences, Kyoto University, Kyoto 606-8501, Japan

Supporting Information

ABSTRACT: The layered compound $SrFeO_2$ with an FeO_4 square-planar motif exhibits an unprecedented pressure-induced spin state transition (S = 2 to 1), together with an insulator-to-metal (I−M) and an antiferromagnetic-to-ferromagnetic (AFM−FM) transition. In this work, we have studied the pressure effect on the structural, magnetic, and transport properties of the structurally related two-legged spin ladder $Sr_3Fe_2O_5$. When pressure was applied, this material first exhibited a structural transition from *Immm* to *Ammm* at $P_s = 30 \pm 2$ GPa. This transition involves a phase shift of the ladder blocks from (1/2,1/2,1/2) to (0,1/2,1/2), by which a rock-salt type SrO block with a 7-fold coordination around Sr changes into a CsCl-type block with 8-fold coordination, allowing a significant reduction of volume. However, the S = 2 antiferromagnetic state stays the same. Next, a spin state transition from S = 2 to S = 1, along with an AFM−FM transition, was observed at $P_c = 34 \pm 2$ GPa, similar to that of $SrFeO_2$. A sign of an I−M transition was also observed at pressure around P_c. These results suggest a generality of the spin state transition in square planar coordinated S = 2 irons of n-legged ladder series $Sr_{n+1}Fe_nO_{2n+1}$ (n = 1, 2, 3, ...). It appears that the structural transition independently occurs without respect to other transitions. The necessary conditions for a structural transition of this type and possible candidate materials are discussed.

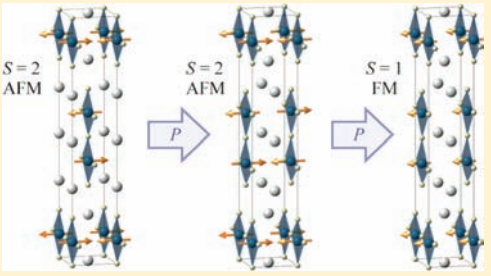

1. INTRODUCTION

Spin state transitions or spin crossover have been intensely investigated in various fields not only for their fundamental details[1] but also because of potential applications in information storage, optical switches, visual displays, and so on.[1,2] Generally, this transition can be rationalized by the competition between the two energies in metal center: the intra-atomic exchange energy that favors a high spin state and the crystal field energy that favors a low spin state.[3,4] Thousands of examples, including minerals and biomolecules, are now found to have spin state transitons,[5−9] but they are almost exclusively limited to those with octahedrally coordinated 3*d* transition metal ions.

A recently discovered pressure-induced spin transition in $SrFe(II)O_2$ at P_c = 33 GPa has several aspects distinct from conventional spin state transitions.[3] First, $SrFeO_2$ adopts a square planar coordination around iron (Figure 1a),[10] thus representing the first spin state transition in a 4-fold coordinated metal center. Second, it is not a typical transition from a high-spin state (S = 2) to a low-spin state (S = 0), but to an intermediate-spin state (S = 1). Last but not least is that it is accompanied at the same time with an insulator-to-metal (I−M) and an antiferromagnetic-to-ferromagnetic (AFM−FM) transition (involving possibly a partial charge transfer from O 2*p* to Fe 3*d* leading to $d^{6.5}$ electronic configurations). These facts indicate that many-body effects derived from the interplay between charge, orbital, and spin degrees of freedom in a strongly correlated electron system are of great importance, which is in stark contrast to conventional cases, where the overall physics behind a spin state transition can be in principle explained by a single (or several) octahedrally coordinated metal(s).

Received: January 15, 2011
Published: March 25, 2011

dx.doi.org/10.1021/ja200410z | *J. Am. Chem. Soc.* 2011, 133, 6036–6043

After the synthesis of $SrFeO_2$, subsequent studies reported several new compounds with the FeO_4 square planar motif; (Sr, Ba,Ca)FeO_2,[11−13] $Sr_3Fe_2O_5$,[14] and $Sr_3Fe_2O_4Cl_2$.[15] Here, $SrFeO_2$ and $Sr_3Fe_2O_5$ belong, respectively, to $n = \infty$ and $n = 2$ of the $S = 2$ n-legged ladder series $Sr_{n+1}Fe_nO_{2n+1}$ ($n = 1, 2, 3, ...$). The former has the infinite layer structure consisting of two-dimensional (2d) FeO_2 layers that are separated by Sr atoms (Figure 1a), whereas in the latter two consecutive rock salt layers (SrO) cut the 2d infinite layers into two-legged ladders ($Sr_2Fe_2O_4$) (Figure 1b). As it is well-known, magnetic and transport properties in a strongly correlated electron system are largely influenced by the topology and dimensionality of the lattice. A representative example is found in the relevant system, $S = 1/2$ n-legged spin ladder series $Sr_{n-1}Cu_nO_{2n-1}$, prepared under high pressures.[16] $SrCuO_2$ ($n = \infty$), whose magnetism is characterized by a square-lattice Heisenberg antiferromagnet, shows a (π, π, π) magnetic order like that of $SrFeO_2$ but becomes a superconductor when appropriate carriers are injected into the CuO_2 plane.[17] The two-legged ladder $SrCu_2O_3$ ($n = 2$) has a nonmagnetic (spin-singlet) ground state with a finite gap to the first excited triplet states, but the three-legged ladder $Sr_2Cu_3O_5$ ($n = 3$) has gapless excitations,[18] verifying a predicted even- or odd-number leg dependence by Dagotto and Rice.[19]

In this context, $Sr_3Fe_2O_5$ provides a unique opportunity to understand how dimensionality is related to the physical properties in the $S = 2$ spin ladder system. The effect of dimensional reduction has been already seen by the reduction of the Néel temperature from $T_N = 473$ K for $SrFeO_2$[3] to $T_N = 296$ K for $Sr_3Fe_2O_5$,[20] but external stimuli such as magnetic field, light and pressure may induce new phenomena. In this paper, we demonstrate the structural, magnetic and transport studies on $Sr_3Fe_2O_5$ under high pressure. We observed a spin state transition from $S = 2$ to $S = 1$, an antiferromagnetic-to-ferromagnetic transition at a nearly identical pressure with $SrFeO_2$. We have also found evidence of an insulator-to-metal transition. These facts indicate the robustness of the transitions to the dimensionality. However, unlike $SrFeO_2$,[3] we observed a structural transition involving a change of a stacking sequence of the ladder blocks.

2. EXPERIMENTAL SECTION

A powder sample of $Sr_3Fe_2O_5$ was synthesized by hydride reaction of a slightly oxygen-deficient $Sr_3Fe_2O_{7-x}$ ($x \sim 0.4$) with CaH_2. The $Sr_3Fe_2O_{7-x}$ precursor was prepared by a high temperature ceramic method from $SrCO_3$ (99.99%), $BaCO_3$ (99.99%) and Fe_2O_3 (99.99%) by heating a pelletized stoichiometric mixture at 1273 K in air for 48 h with one intermediate grinding. For reduction, $Sr_3Fe_2O_{7-x}$ and a four molar excess of CaH_2 were finely ground in an Ar-filled glovebox, sealed in an evacuated Pyrex tube, and heated at 598 K for 1 day. Residual CaH_2 and the CaO byproduct were removed from the final reaction phase by washing them out with an NH_4Cl/methanol solution. For more details, refer to the literature.[14] In order to obtain better statistics for the ^{57}Fe Mössbauer spectroscopy measurements, ^{57}Fe-enriched $Sr_3Fe_2O_5$ (^{57}Fe consisting of about 50% of the total Fe amount) was prepared.

The high-pressure ^{57}Fe Mössbauer measurements were performed up to 100 GPa using a Bassett-type diamond-anvil cell (DAC).[21] The powder sample and small ruby chips were inserted in a 200 μm hole of a Re gasket. Daphne7474 was used as a pressure-transmitting medium. A point γ-ray source of ^{57}Co in a rhodium matrix of 370 MBq and another one of 925 MBq with active areas of 1 mm and 5 mm in diameter, respectively, were used. The velocity scale of the spectrum was relative to α-Fe at room temperature (RT). We estimated the pressure distribution

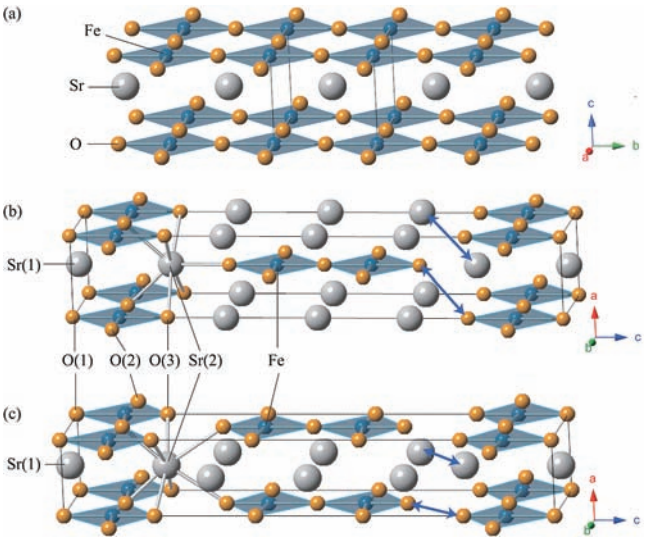

Figure 1. Comparison of the structure of (a) $SrFeO_2$ and $Sr_3Fe_2O_5$ at (b) low pressure ($P < P_s$) and (c) high pressure ($P_s < P$). White, blue, and orange spheres represent Sr, Fe, and O atoms, respectively. Blue arrows represent the adjacent Sr(2)−Sr(2) and O(2)−O(2).

along the sample by measuring fluorescence of ruby chips dispersed in the sample, as shown in Figure 1S in Supporting Information. We found that the pressure gradient at the sample was not more than 5 GPa at maximal pressures. Experiments under the external magnetic field up to 3 T were carried out with the magnetic field applied along the γ-ray propagation direction. For examination of the intermediate-pressure phase, we employed a DAC with a 180 μm hole of a Re gasket in order to obtain a smaller pressure gradient.

Four-probe dc resistance measurements up to 67 GPa were carried out between 5 and 300 K with Pt electrodes. The sample/metal-gasket cavity was coated with an insulating mixture of Al_2O_3 and NaCl combined with epoxy. The initial sectional area and the distance between probes were about 60 × 50 μm^2 and 50 μm. Applied pressure was calibrated by means of fluorescence manometer on ruby chips placed around the sample.

Powder X-ray diffraction (XRD) profiles at high pressures up to 39 GPa at RT were recorded using Mo K_α radiation from a 5.4 kW Rigaku rotating anode generator equipped with a 100 μm collimator. A powder sample of $Sr_3Fe_2O_5$ was loaded into a 180 μm diameter hole of a preindented rhenium gasket of the diamond-anvil cell. Helium was used as a pressure-transmitting medium. The shift of ruby fluorescence was used to determine the pressure. The pressure gradient at the sample increased slowly with pressure but was not more than 0.5 GPa at the maximum pressure. The diffracted X-rays were collected with an imaging plate. More details of the experimental setup are reported elsewhere.[22] Three diffraction peaks, (015), (105), (110) for the low-pressure phase and (015), (104), (111) for the high-pressure phase, were used to obtain the cell parameters.

High-resolution synchrotron XRD experiments at high pressures up to 36.7 GPa were performed at RT using angle-dispersive X-ray diffractometry installed in the NE1 synchrotron beamline of the Photon Factory-Advanced Ring for Pulse X-rays (PF-AR) at the High Energy Accelerator Research Organization (KEK), Japan. The incident X-ray beam was monochromatized to a wavelength of 0.41310 Å. The X-ray beam size was collimated to a diameter of about 50 μm. The angle-dispersive X-ray diffraction patterns were obtained on an imaging plate. The pressure gradient at the sample, estimated in the same way as described above, was not more than 1.0 GPa at maximal pressures. The observed intensities on the imaging plates were integrated as a function

dx.doi.org/10.1021/ja200410z |J. Am. Chem. Soc. 2011, 133, 6036–6043

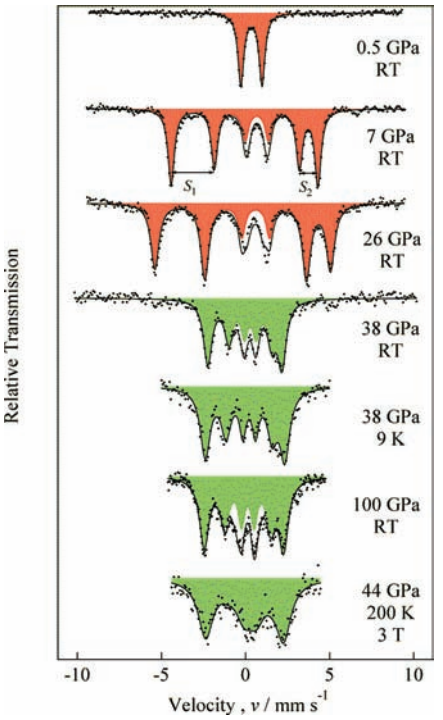

Figure 2. Observation of the spin state transition in $Sr_3Fe_2O_5$ by high-pressure ^{57}Fe Mössbauer experiments. The red spectra correspond to the $S = 2$ state, and the green correspond to the $S = 1$ state. The solid lines represent the total fitted curves. The difference between the first and second peaks and the fifth and sixth peaks, S_1-S_2, represents QS (see text for more detail).

of 2θ using the Fit2d code[23] to obtain conventional, one-dimensional diffraction profiles. The obtained synchrotron XRD data were analyzed by the Rietveld method using RIETAN-FP program.[24]

3. RESULTS AND DISCUSSIONS

Typical ^{57}Fe Mössbauer spectra at high pressures are shown in Figure 2. At 0.5 GPa, the spectrum at RT consists of doublet peaks with an isomer shift IS of 0.47 mm/s and a quadrupole splitting QS of 1.26 mm/s, indicating a paramagnetic state as well as square-planar coordination geometry for a high-spin Fe^{2+}, which is consistent with a previous study.[14] When more pressure was applied at RT, the doublet immediately changed to six well-defined peaks, indicating the presence of magnetic order. The value of S_1-S_2 as indicated in the spectrum at 7 GPa of Figure 2 is 1.48 mm/s, which is very close to the QS value at 0.5 GPa in the paramagnetic state. A gradual and linear decrease in IS with pressure (Figure 3) is in accordance with the trend observed in many iron compounds including $SrFeO_2$[3,5] and can be interpreted in terms of a gradually increased hybridization of iron 3d orbitals with the 2p orbitals of the oxygen neighbors.

With increasing pressure up to 30 GPa, the split of the sextet increases (see the 26 GPa spectrum in Figure 2), implying the increase of T_N, which should result from increased magnetic interactions through the decrease of cell parameter. Indeed, the temperature-dependent Mössbauer measurements at pressures up to 10 GPa reveals that T_N has a linear increase with pressure in this pressure region (Figure 4 and Figure 2S in Supporting Information). One can see from the top panel of Figure 3 that the hyperfine field H_{hf} steeply increases up to 10 GPa as anticipated

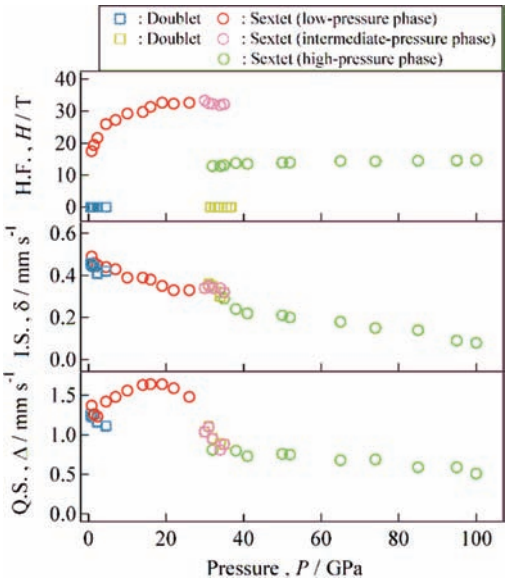

Figure 3. Pressure dependence of Mössbauer parameters of $Sr_3Fe_2O_5$: H_{hf} (top), IS (middle), and QS (bottom) at RT.

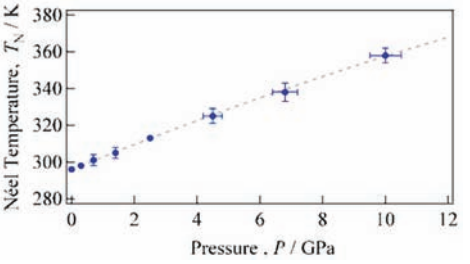

Figure 4. Pressure dependence of T_N as determined by the ^{57}Fe Mössbauer spectra at elevated temperatures.

but then saturates above 20 GPa to ~32 T. This value is much smaller than 43.7 T at 4 K in an ambient pressure (corresponding to the fully saturated moment for $S = 2$)[14] and 41.6 T at 4 K and 23 GPa (Figure 3S in Supporting Information). The tendency of T_N to saturate above 20 GPa is not consistent with the pressure dependence of the cell parameters. All of the crystallographic axes continuously decrease with pressure as will be shown later. At 10 GPa, T_N rises up to 365 K (22% increase with respect to the ambient pressure data). Remarkably, H_{hf} for $SrFeO_2$ is nearly independent of both pressures[3] and Sr-to-Ca substitution (ref 12 and unpublished data), despite the fact that a and c in $SrFeO_2$[3] and a and b in $Sr_3Fe_2O_5$ (as will be shown later) behave similarly as a function of pressure before the transition arrives, as shown in Figure 6b. The variability of T_N for $Sr_3Fe_2O_5$ with pressure can be explained in terms of geometrical frustration in the ladder arrangement due to the I-centered lattice.

The spectrum at 7 GPa contains a small portion of a doublet with IS and QS values (0.64 and 1.41 mm/s, respectively) similar to those of the sextet (0.42 and 1.48 mm/s), as seen in Figure 2. The doublet-to-sextet ratio slightly increases at 26 GPa. At each pressure measured in this study, the doublet vanishes at 9 K so that this component is not considered to arise from impurity phase but from $Sr_3Fe_2O_5$ having a lower T_N (T_N < RT). Note that we did not observe such a coexistence with a paramagnetic

dx.doi.org/10.1021/ja200410z |J. Am. Chem. Soc. 2011, 133, 6036–6043

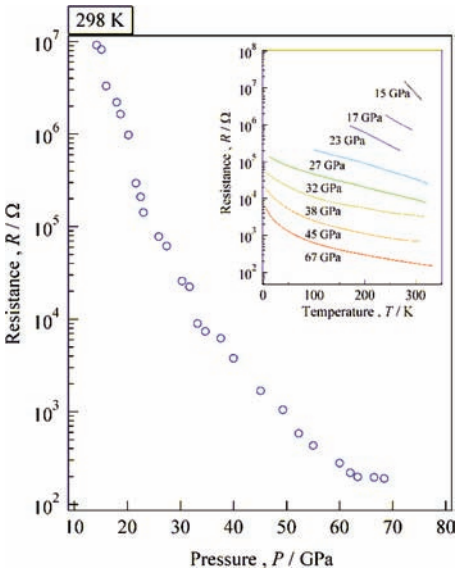

Figure 5. Room temperature electrical resistance as a function of *P*. Inset shows temperature dependence of the electrical resistance under high pressure.

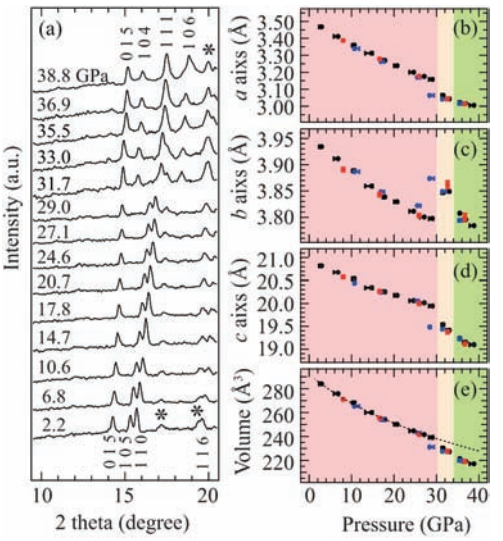

Figure 6. (a) Powder XRD patterns of $Sr_3Fe_2O_5$ at various pressures at RT, indexed on the orthorhombic unit cell. Asterisks correspond to peaks from rhenium. Pressure dependence of (b−d) the lattice parameters and (e) the volume. Black circles represent the data obtained upon increasing pressure using laboratory XRD, blue circles represent those obtained upon releasing pressure using laboratory XRD, and red circles represent those obtained using synchrotron XRD. The dotted line in panel (e) represents Birch−Murnaghan fitting below P_s.

component in the previous high-pressure study of $SrFeO_2$.[3] This means that a structural strain caused by nonhydrostatic stress would be more prominent in $Sr_3Fe_2O_5$ than in $SrFeO_2$. Under our experimental conditions, solidification of a pressure medium (Daphne7474) inevitably results in nonhydrostatic pressure to the $Sr_3Fe_2O_5/SrFeO_2$ samples. Given the intergrowth structure composed of different units (i.e., rock-salt and ladder blocks), such an effect in $Sr_3Fe_2O_5$ would be much stronger than in $SrFeO_2$. Even a small amount of strain might cause a substantial reduction of T_N due to the geometrical frustration in the magnetic lattice as already pointed out.

When further pressure was applied, a drastic change in the Mössbauer spectra appeared (see Figure 2), featured by a reduction of the hyperfine field (H_{hf} = 13.5 T at 38 GPa, RT), suggesting an intermediate-spin (S = 1) state as was observed in the high-pressure phase of $SrFeO_2$.[3] When the sample was cooled to 9 K, H_{hf} is increased to 18.4 T, which is nearly half of that of the low-pressure phase, thereby confirming that the iron ions are in the intermediate spin state. Figure 3 shows that the obtained *IS* and *QS* values are close to those of the intermediate-spin state of $SrFeO_2$,[3] demonstrating that the iron is in a square planar geometry having only one crystallographically equivalent site. The relatively large H_{hf} value in the intermediate-spin state at RT indicates well-developed magnetic order. Despite the pressure gradient of ∼5 GPa, a careful analysis of the relative spectrum weight gave a rough estimate of the transition pressure P_c as 34 ± 3 GPa, which is surprisingly close to that of $SrFeO_2$.[3] When a magnetic field was applied parallel to the γ ray direction, the intensities of the second and fifth lines of the sextet at 44 GPa showed a remarkable decrease at 1.5 T (not shown) and disappeared at 3 T (see Figure 2), indicating that the high-pressure phase ($P > P_c$) is a FM state. The AFM−FM transition at P_c was also found in $SrFeO_2$.[3] The spectral features of the S = 1 state remain up to the maximum pressure of 100 GPa applied in this study. This shows that the S = 1 FM state is quite robust, as in the case of $SrFeO_2$.[3]

Given the high-spin to intermediate-spin state transition and the AFM-to-FM transition in $Sr_3Fe_2O_5$, an I−M transition, which was observed in $SrFeO_2$,[3] is intuitively expected. The electrical resistivity of $Sr_3Fe_2O_5$ performed under pressure is shown in Figure 5. The resistivity is unmeasurably high below 15 GPa, due to a large band gap as theoretically suggested.[25] However, it became measurable above 15 GPa and then remarkably decreases. It is reduced by 5 orders of magnitude at 60 GPa. Such a large decrease in the resistivity suggests the presence of an I−M transition at P_c, although the temperature dependence of the electrical resistance ($\Delta R/\Delta T$) does not become positive even at 67 GPa. It should be noted that the observation of metallic behavior ($\Delta R/\Delta T > 0$) in a powder sample is in general difficult in low dimensional materials as demonstrated by $Na_{1/3}V_2O_5$.[26] Moreover, the obscurity of the transition may be a result of surface damage due to the air sensitivity of $Sr_3Fe_2O_5$[14] and pressure inhomogeneity. It is well-known that divalent iron oxides are all insulators.[27,28] According to first principles calculations, the unusual metallic state of $SrFeO_2$ under high pressure is accompanied by the charge transfer from O 2*p* to Fe 3*d*, resulting in d^6 to $d^{6.5}$ electronic configurations.[3] Accordingly, it is natural to expect that the electric conductivity in $Sr_3Fe_2O_5$ is also attributed to the charge transfer. However, despite such evidence pointing toward an I−M transition, the resistivity data is still ambiguous, and first principles calculations for $Sr_3Fe_2O_5$ would shed more light on this issue.

A pressure-induced spin state transition always involves a volume reduction at P_c.[3,9] In order to probe this, we carried out high pressure XRD experiments at RT up to 38.8 GPa (see Figure 6a). In $SrFeO_2$, we previously reported that the diffraction patterns do not show any spectacular change at P_c; the anomaly at P_c is recognizable only when the cell parameters are plotted as a function of *P*.[3] In the case of $Sr_3Fe_2O_5$, however, we unexpectedly found a drastic change in the diffraction pattern above 30 GPa. From *P* = 2.2 to 29.0 GPa, all diffraction peaks (excluding rhenium peaks) could be assigned to an *I*-centered orthorhombic

dx.doi.org/10.1021/ja200410z |*J. Am. Chem. Soc.* 2011, 133, 6036–6043

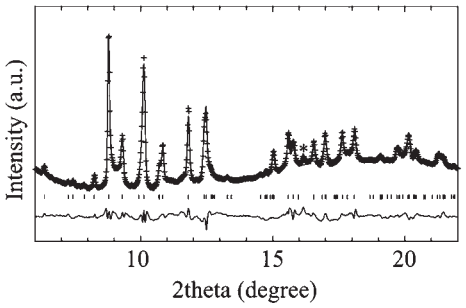

Figure 7. Structural characterization of $Sr_3Fe_2O_5$ by the Rietveld refinement of the synchrotron XRD data at 36.7 GPa and RT. The overlying crosses and the solid line represent the observed and the calculated intensities. The bottom solid line represents the difference between the observed intensity and the calculated intensity. The ticks correspond to the position of the calculated Bragg peaks of high-pressure phase of $Sr_3Fe_2O_5$. Asterisk indicates reflection from unknown impurity.

structure. The diffraction patterns above 30 GPa could be also indexed on the basis of the orthorhombic unit cell (e.g., a = 3.00 Å, b = 3.78 Å, c = 19.09 Å at 38.8 GPa) but have different extinction conditions. It is seen from Figure 6a, for example, that the originally extinct (104) and (111) peaks in the low-pressure structure (space group *Immm*) appear, while the originally allowed (105) and (110) peaks disappear. It follows that the new structure induced by pressure has an *A*-centered orthorhombic lattice. When releasing the pressure, the high-pressure structure remained at pressures above 28.4 GPa and then completely returned to the original low-pressure structure at pressures below 25.5 GPa (see Figure 4S in Supporting Information) without any loss in crystallinity, suggesting that the structural transition is of first-order, reversible and topotactic.

As depicted in Figure 6b−d, all of the axes decrease smoothly before the structural transition arrives. The pressure dependence of the volume for the low-pressure structure (Figure 6e) can be fitted well by the Birch−Murnaghan equation of the state,[29] yielding the bulk modulus of K = 94 GPa, which is slightly smaller than that of $SrFeO_2$ (K = 126 GPa).[3] The volume reduction at 30 GPa is about 4%. Remarkably, while the a and c axes decrease during this transition, the b axis (i.e., the leg direction) increases. Due to the small pressure distribution within the sample (<0.5 GPa) for the XRD experiments, the structural transition pressure P_s can be precisely determined as 30 ± 2 GPa based on the data during compression. In the case of $SrFeO_2$, we employed almost the same experimental setup as the present study and obtained a perfect agreement of P_c,[3] at which the anomaly was found in Mössbauer (33 ± 3 GPa) and XRD (33 ± 1 GPa) measurements, but in $Sr_3Fe_2O_5$ there is an apparent discrepancy between P_s (= 30 ± 2 GPa) obtained from the XRD measurements and P_c (= 34 ± 3 GPa) obtained from the Mössbauer measurement, a strong indication that the structural transition and the spin state transition are independent. In support of this interpretation, we see a large drop of the b axis at 34 ± 2 GPa (see Figure 6c), which coincides with P_c. The volume reduction at P_c is as much as 3%. The presence of the intermediate phase (i.e., the two critical pressures at 30 and 34 GPa) was further confirmed by careful Mössbauer measurements as discussed later.

The high-pressure structure up to 36.7 GPa was determined using synchrotron XRD data (Figures 7 and 5S in Supporting Information). As expected, the XRD patterns measured above P_s could be indexed on the *A*-centered orthorhombic cell

Table 1. Structural Parameters for $Sr_3Fe_2O_5$ at 36.7 GPa Obtained by Rietveld Refinement[a]

atom	site	g	x	y	z	B, Å^2
Sr(1)	2*c*	1	0.5	0.5	0	0.4(2)
Sr(2)	4*j*	1	0.5	0.5	0.1979(3)	0.4(2)
Fe	4*i*	1	0	0	0.1029(7)	1.5(2)
O(1)	2*a*	1	0	0	0	0.6(4)
O(2)	4*i*	1	0	0	0.386(2)	0.6(4)
O(3)	4*i*	1	0	0	0.188(3)	0.6(4)

[a] Space group: *Ammm*, a = 3.0108(4) Å, b = 3.8004(4) Å, c = 19.113(3) Å. R_{wp} = 0.90%, R_p = 0.66%, χ^2 = 0.89. R_{Bragg} = 4.98%, R_F = 3.28%.

(a = 3.014(4) Å, b = 3.800(7) Å, c = 19.11(3) Å at 36.7 GPa), and several small reflections from unknown impurities were found. Earlier, we already explained from the Mössbauer spectra that the irons in the high-pressure structure are in a square planar geometry having only one crystallographically equivalent site. In addition, the structural transition is reversible with only small hysteresis, indicating that the two structures are topotactically related with each other. All of these observations led us to consider that the structural transition from the *I*- to *A*-centered space group is caused by a change in the stacking sequence of the two-legged ladder (or the original perovskite) blocks. In the *I*-centered structure of $Sr_3Fe_2O_5$ below P_s (or that of its precursor $Sr_3Fe_2O_7$), the two-legged ladder (or perovskite) blocks are phase-shifted from each other by (1/2, 1/2, 1/2) (see Figure 1b). In the *A*-centered structure above P_s, we expected that the adjacent ladder blocks are staggered only in the b and c directions, giving a phase shift of (0, 1/2, 1/2) as shown in Figure 1c.

Possible space groups for the high-pressure phase are *Ammm*, *A*2*mm*, *Am*2*m*, *Amm*2, and *A*222. Among these candidates, *Ammm* is the maximal nonisomorphic subspace group for *Immm*, the space group for the low-pressure structure. Accordingly, we chose *Ammm* as the initial space group for refinement of the high-pressure structure. Assuming Sr(1) to be at 2*c* (0.5, 0.5, 0), Sr(2) at 4*j* (0.5, 0.5, z), Fe at 4*i* (0, 0, z), O(1) at 2*a* (0, 0, 0), O(2) at 4*i* (0, 0, z) and O(3) at 4*i* (0, 0, z), we refined the structural parameters while the occupancy factors were constrained to unity. The refinements converged well, providing R_{wp} = 0.90%, χ^2 = 0.89 (see Figure 7). These small agreement indices as well as the small atomic displacement parameters B for all atoms suggest that the refined structure is reasonable. Other candidate space groups with lower symmetry did not give any appreciable improvement in the structural refinement, so we conclude that the structure with *Ammm* as summarized in Table 1 is the best choice.

The interatomic distances for the refined structure are listed in Figure 8 and Table 2. The FeO_4 square planar coordination at ambient pressure consists of four almost equivalent bonds (∼2.0 Å), while that at 36.7 GPa has a distortion with three long bonds (1.97(1) Å and 1.912(5)Å) and one short bond (1.62(5) Å), as shown in Figure 8. The mean Fe−O distance of 1.85 Å is close to that for $SrFeO_2$ at 39.2 GPa (1.88 Å). The Sr−O distance at 36.7 GPa ranges from 2.20 to 2.65 Å, which is acceptable in this pressure region considering previous studies.[3,30−32] As for Sr(1), Sr(2) is 8-fold coordinated to oxygen atoms in the CsCl-type structure (Figures 1c and 8). The mean bond distance around Sr(1) (2.53 Å) is slightly longer than that for $SrFeO_2$ at 39.2 GPa (2.41 Å). However, that of Sr(2) (2.43 Å) is very close to 2.41 Å.

We see now that $Sr_3Fe_2O_5$ undergoes a pressure-induced structural transition involving a phase shift of the two-legged

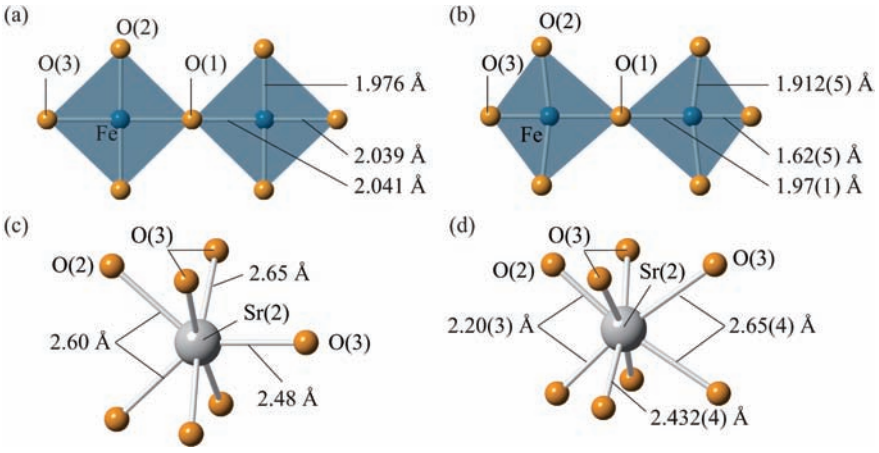

Figure 8. Coordination around Fe and Sr(2). (a) Iron coordination in the low-pressure structure at ambient pressure,[14] and (b) the high-pressure structure at 36.7 GPa. (c) Sr(2) coordination in the low-pressure structure at ambient pressure,[14] and (d) the high-pressure structure at 36.7 GPa.

Table 2. Interatomic Distances for $Sr_3Fe_2O_5$ at 36.7 GPa

	distance (Å)
Sr(1)−O(1) × 4	2.4243(2)
Sr(1)−O(2) × 4	2.65(4)
Sr(2)−O(2) × 2	2.20(3)
Sr(2)−O(3) × 2	2.65(4)
Sr(2)−O(3) × 4	2.432(4)
Fe−O(1) × 1	1.97(1)
Fe−O(2) × 2	1.912(5)
Fe−O(3) × 1	1.62(5)

ladder blocks. The change of the stacking sequence at P_s leads to the increase of the oxygen coordination number of Sr(2) from seven to eight (see Figure 1b and c), while maintaining the FeO_4 square planar coordination. The new structure adopts the intergrowth of a two-legged ladder with CsCl-type structure. In geology, the structural transition from the *B*1(NaCl) type to the *B*2(CsCl) type was intensively studied by both theoretical[33,34] and experimental[35,36] methods due to the possible occurrence of this transition in the earth's lower mantle, which could affect the transmission of seismic waves. Indeed, *AX* materials (*A* = Be, Mg, Ca, Sr, Ba, *X* = O, S, Se, Te) with the *B*1 structure undergo or are predicted to undergo structural transitions to the *B*2 structure with observed or expected critical pressures ranging from 5 to 1000 GPa, depending on the ionic radii of *A*.[35−37] In SrO, the *B*1 to *B*2 transition occurs at 36 GPa which is close to P_s (= 30 GPa) observed in $Sr_3Fe_2O_5$.[38] Moreover, the atomic distances (Sr−Sr, O−O and Sr−O) of the two compounds above P_s are similar; those of SrO at 37 GPa are, respectively, 2.89, 2.89 and 2.50 Å while Sr(2)−Sr(2), O(3)−O(3) and the mean Sr(2)−O distance of $Sr_3Fe_2O_5$ at 36.7 GPa are 2.752(7), 3.05(6) and 2.43 Å. All of these facts validate the observed transition in $Sr_3Fe_2O_5$. It is also interesting to point out that Dion−Jacobson-type layered perovskite oxides $ALaNb_2O_7$ (*A* = alkali metal) exhibit a similar structural modification,[39] where the stacking sequence of the perovskite blocks can be varied by the ionic radius of the *A* ion, instead of pressure. *A* = Cs, K and Li, respectively, give *P*-, *A*-, *I*-centered structures with 8, 6 and 4-fold coordination around the *A* ion, while maintaining the perovskite blocks (Figure 6S in Supporting Information).

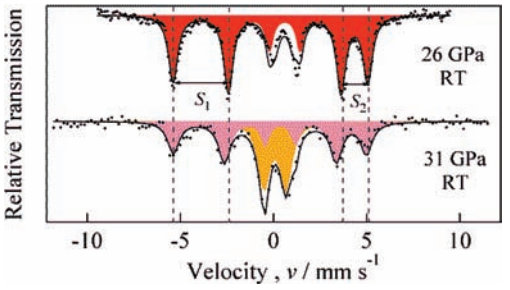

Figure 9. ^{57}Fe Mössbauer spectra in the *S* = 2 state at RT. The red spectrum corresponds to the low-pressure phase, and the pink and orange correspond to the intermediate-pressure phase.

The new structure above P_s consists of *infinite* Fe_2O_5 layers intervened by Sr atoms along the *a* direction with the sequence [-Fe_2O_5-Sr_3-Fe_2O_5-Sr_3-] (Figure 1c). In the low-pressure structure (Figure 1b), each Fe_2O_7 rung is collinearly aligned with the neighboring Sr(2) atoms along [001], whereas in the high-pressure phase each Fe_2O_7 rung is connected to two Fe_2O_7 rungs of neighboring ladders in a zigzag manner. It is this staggered arrangement that permits a distinct decrease of *c* during the structural transition (∼0.4 Å). Also, the alternating stacking of $(Fe_2O_5)^{6-}$ and $(Sr_3)^{6+}$ in the high-pressure structure would effectively reduce the stack distance along the *a* axis (Δa ∼0.1 Å). On the contrary, the large reduction in *a* and *c* axes by the phase shift is partly compensated by the increase of the *b* axis (the leg direction) of about ∼0.05 Å. The elongation of this axis is rationalized as the relief of coulomb repulsion between adjacent Sr(2) ions and between adjacent O(1) ions (see the arrows in Figure 1), both of which become considerably shorter upon the structural transition (Sr(2)−Sr(2): 3.5 → 2.8 Å; O(1)−O(1): ∼3.3 → ∼3.1 Å).

There remains a question about magnetic properties of the intermediate-pressure phase ($P_s < P < P_c$). Thus we decided to perform Mössbauer measurements in this pressure region using a different batch. In this measurement, we used a DAC with the smaller sample hole in order to obtain a smaller pressure gradient. As shown in Figure 9, the RT spectrum at 31 GPa consists of sextet (57%) and doublet (43%). The H_{hf} for the sextet component is 32.4 T at RT and is 40.2 T at 4 K (Figure 3S in Supporting Information), indicating persistence of the high-

dx.doi.org/10.1021/ja200410z |*J. Am. Chem. Soc.* 2011, 133, 6036–6043

spin state, but we notice that S_1-S_2 (1.10 mm/s) is different from that at 26 GPa (see Figure 9) and is rather close to those at $P > P_c$ as demonstrated in Figure 3. Since QS ($= S_1 - S_2$) provides relevant information on the local structure around iron, the sextet component can be assigned as intrinsic to the intermediate-pressure phase ($P_s < P < P_c$). The doublet component has nearly the same *IS* and *QS* values as the sextet at 31 GPa so that it is also ascribed as intrinsic to the intermediate-pressure phase. We deduce that structural strains induced by the structural transition might be a possible reason why the spin-ordered coexists with the disordered states in the intermediate-pressure phase.

The low-temperature spectrum at 31 GPa consists of only a single set of sextet (Figure 3S in Supporting Information), meaning that the paramagnetic phase also experiences magnetic order. By the application of magnetic field of 3 T, the sextet becomes markedly broadened, which indicates that the intermediate-pressure phase is in an AFM state as the low-pressure phase (Figure 3S in Supporting Information). The magnetic moments align parallel to the FeO_4 square planar unit, as in the low-pressure $S = 2$ AFM and high-pressure $S = 1$ FM phases. It is not possible to determine the magnetic structure of the intermediate AFM phase from the Mössbauer data, but the *G*-type order as observed at ambient pressure[14] is likely to be preserved because a change in the spin structure in $SrFeO_2$ takes place together with the spin state transition.

It is interesting that the spin state transition in $Sr_3Fe_2O_5$ occurs at almost the same pressure as $SrFeO_2$,[3] an observation pointing out that the dimensionality has little influence on the spin state transition. Whangbo and Köhler argued that the face-to-face FeO_4 square planar arrangement is essential for the occurrence of the spin state transition in $SrFeO_2$.[4] In accordance with their argument, $Sr_3Fe_2O_5$ containing the same face-to-face arrangement exhibits the spin state transition. However, close inspections of the structures of $SrFeO_2$ and $Sr_3Fe_2O_5$ have found several aspects to be addressed. First, the distance between adjacent face-to-face FeO_4 square planar units (i.e., a for $Sr_3Fe_2O_5$ and c for $SrFeO_2$) is considered as the most crucial factor for the spin state transition, but the spin state transition occurs when $c = 3.09$ Å for $SrFeO_2$ and $a = 3.04$ Å for $Sr_3Fe_2O_5$. The structural transition helps to shorten a, and the length at P_s is close to c for $SrFeO_2$ at P_c. The second concerns the shape of the FeO_4 square planar coordination; in $SrFeO_2$ all four Fe−O bonds are equal in length,[3] but this is not the case in $Sr_3Fe_2O_5$ below P_s, and further distortion becomes more prominent above P_s (Figure 8). Owing to the short Fe−O(1) length, the iron atom is shifted toward O(3), which results in a deviation of the Fe−O(2)−Fe bridging angle from the ideal value 180° (e.g., 167° at 36.7 GPa). Third, the *d*-orbital occupation and electronic configuration should be affected by the deformed structure of FeO_4. In the $S = 1$ state of $SrFeO_2$, the d_{xy} and d_{yz} for the spin-down channel are equally filled (half-filled),[3] but this balance might be disturbed in $Sr_3Fe_2O_5$. All these factors can more or less contribute to changing P_c, so that it is possible that our observation can be a mere accidental coincidence. Therefore, a systematic and comprehensive study of the other ladder series $Sr_{n+1}Fe_nO_{2n+1}$ including Sr_2FeO_3 and $Sr_4Fe_3O_7$ (not yet synthesized) is strongly desired.

As demonstrated already, the structural transition in $Sr_3Fe_2O_5$ can be explained quite adequately by structural terms so that we consider that the two transitions occur independently (although the proximity of P_s and P_c in $Sr_3Fe_2O_5$ superficially suggests some interplays between them). If this is the case, we can in turn predict a pressure-induced structural transition for compounds that share structural features with $Sr_3Fe_2O_5$. Among the candidate materials are A_2CuO_3 (A = Ca, Sr, Ba)[40,41] and Sr_2PdO_3,[42] all having the *Immm* space group with the intergrowth structure of *A*O rock-salt block and CuO_2 (PdO_2) chain (or one-legged ladder) blocks, being isostructural with the hypothetical compound Sr_2FeO_3. Another candidate, K_2NiO_2, is tetragonal (*I*4/*mmm*), which differs from the aforementioned A_2CuO_3 structure by the absence of bridging oxygen, yielding a 2-fold dumbbell coordination around Ni.[43] It is interesting to check whether the orthorhombicity is necessary or not for the structural transition from the *I*- to *A*-centered lattice.

4. CONCLUSION

$Sr_3Fe(II)_2O_5$ exhibits a spin state transition from $S = 2$ to $S = 1$ state at $P_c = 34$ GPa with an AFM−FM transition. Signs suggesting an I−M transition were also observed at pressure around P_c. $SrFeO_2$ shows the same behavior, suggesting a general intrinsic character for square planar coordinated iron oxides. The critical pressure P_c is insensitive to the dimensionality, but further studies especially using other systems $Sr_{n+1}Fe_nO_{2n+1}$ are needed to understand the spin-ladder physics for $S = 2$. Most importantly, unlike $SrFeO_2$, we also observed a pressure-induced structural transition at $P_s = 30$ GPa, which involves a change in the stacking sequence of the ladder blocks. The SrO block of the original 7-fold rock-salt structure adopts the 8-fold CsCl structure. This allows an efficient contraction of the volume. Ever since the prediction of superconductivity in the $S = 1/2$ two-legged ladder system by Dagotto et al.,[44] the search for superconductivity has been vigorously performed and $(Sr_{1-x}Ca_x)_{14}Cu_{24}O_{41}$ was found to show superconductivity under high-pressure although its T_c is low.[45] The successful metallization of $S = 2$ $Sr_3Fe_2O_5$ under high pressure would also provides hope that further pressurization could lead to superconductivity.

■ ASSOCIATED CONTENT

Supporting Information. Experimental details and characterization data for the new compounds and complete ref 3. This material is available free of charge via the Internet at http://pubs.acs.org.

■ AUTHOR INFORMATION

Corresponding Author
kage@scl.kyoto-u.ac.jp

Present Addresses
Permanent address: Department of Energy and Hydrocarbon Chemistry, Graduate School of Engineering, Kyoto University, Kyoto 615−8510, Japan.

■ ACKNOWLEDGMENT

We thank Drs. R. Podloucky, Xing-Qiu Chen, N. Hayashi, Y. Tsujimoto, and Y. Ajiro for helpful discussions. This work was supported by Grants-in-Aid for Science Research in the Priority Areas "Novel States of Matter Induced by Frustration" (No. 19052004) and by Grant-in-Aid for Scientific Research (A) (No. 22245009) from the Ministry of Education, Culture, Sports, Science and Technology of Japan, the Global COE program International Center Science, Kyoto University, Japan, and by

the Japan Society for the Promotion of Science (JSPS) through its "Funding Program for World-Leading Innovative R&D on Science and Technology (FIRST) Program". T.Y. was supported by the Japan Society for the Promotion of Science for Young Scientists. T.K. acknowledges partial support from the Foundation "Hattori-Hokokai" and "Strategic Research Base Development" Program for Private Universities subsidized by MEXT (2009, S0901022).

■ ADDITIONAL NOTE

For each phase of $Sr_3Fe_2O_5$, the Fe spins are oriented within the FeO_4 plane, however, in the abstract graphic, they have been drawn perpendicular to the FeO_4 plane for clarity.

■ REFERENCES

(1) Gütlich, P.; Hauser, A.; Spiering, H. *Angew. Chem., Int. Ed.* **1994**, *33*, 2024–2054.
(2) Kahn, O.; Martinez, C. J. *Science* **1998**, *279*, 44–48.
(3) Kawakami, T.; et al. *Nat. Chem.* **2009**, *1*, 371–376.
(4) Whangbo, M. H.; Köhler, J. *Nat. Chem.* **2009**, *1*, 351–352.
(5) Takano, M.; Nasu, S.; Abe, T.; Yamamoto, K.; Endo, S.; Takeda, Y.; Goodenough, J. B. *Phys. Rev. Lett.* **1991**, *67*, 3267–3270.
(6) Abbate, M.; Fuggle, J. C.; Fujimori, A.; Tjeng, L. H.; Chen, C. T.; Potze, R.; Sawatzky, G. A.; Eisaki, H.; Uchida, S. *Phys. Rev. B.* **1993**, *47*, 16124–16130.
(7) Real, J. A.; Andrés, E.; Muñoz, M. C.; Julve, M.; Granier, T.; Bousseksou, A.; Varret, F. *Science* **1995**, *268*, 265–267.
(8) Halder, G. J.; Kepert, C. J.; Moubaraki, B.; Murray, K. S.; Cashion, J. D. *Science* **2002**, *298*, 1762–1765.
(9) Lin, J. F.; Struzhkin, V. V.; Jacobsen, S. D.; Hu, M. Y.; Chow, P.; Kung, J.; Liu, H.; Mao., H. K.; Hemley, R. J. *Nature* **2005**, *436*, 377–480.
(10) Tsujimoto, Y.; Tassel, C.; Hayashi, N.; Watanabe, T.; Kageyama, H.; Yoshimura, K.; Takano, M.; Ceretti, M.; Ritter, C.; Paulus, W. *Nature* **2007**, *450*, 1062–1065.
(11) Tassel, C.; Watanabe, T.; Tsujimoto, Y.; Hayashi, N.; Kitada, A.; Sumida, Y.; Yamamoto, T.; Kageyama, H.; Takano, M.; Yoshimura, K. *J. Am. Chem. Soc.* **2008**, *130*, 3764–3765.
(12) Tassel, C.; Pruneda, J. M.; Hayashi, N.; Watanabe, T.; Kitada, A.; Tsujimoto, Y.; Kageyama, H.; Yoshimura, K.; Takano, M.; Nishi, M.; Ohoyama, K.; Mizumaki, M.; Kawamura, N.; Íñiguez, J.; Canadell, E. *J. Am. Chem. Soc.* **2009**, *131*, 221–229.
(13) Yamamoto, T.; Li, Z.; Tassel, C.; Hayashi, N.; Takano, M.; Isobe, M.; Ueda, Y.; Ohoyama, K.; Yoshimura, K.; Kobayashi, Y.; Kageyama, H. *Inorg. Chem.* **2010**, *49*, 5957–5962.
(14) Kageyama, H.; Watanabe, T.; Tsujimoto, Y.; Kitada, A.; Sumida, Y.; Kanamori, K.; Yoshimura, K.; Hayashi, N.; Muranaka, S.; Takano, M.; M. Ceretti, K.; Paulus, W.; Ritter, C. *Angew. Chem., Int. Ed.* **2008**, *47*, 5740–5745.
(15) Dixon, E.; Hayward, M. A. *Inorg. Chem.* **2010**, *49*, 9649–9654.
(16) Hiroi, Z.; Azuma, M.; Takano, M.; Bando, Y. *J. Solid State Chem.* **1991**, *95*, 230–238.
(17) Smith, M. G.; Manthiram, A.; Zhou, J.; Goodenough, J. B. *Nature* **1991**, *351*, 549–551.
(18) Azuma, M.; Hiroi, Z.; Takano, M.; Ishida, K.; Kitaoka, Y. *Phys. Rev. Lett.* **1994**, *73*, 3463–3466.
(19) Dagotto, E.; Rice, T. M. *Science* **1996**, *271*, 618–623.
(20) Hayashi, N.; Kageyama, H.; Tsujimoto, Y.; Watanabe, T.; Muranaka, S.; Ono, T.; Nasu, S.; Ajiro, Y.; Yoshimura, K.; Takano, M. *J. Phys. Soc. Jpn.* **2010**, *79*, 123709.
(21) Bassett, W. A.; Takahashi, T.; Stook, P. W. *Rev. Sci. Instrum.* **1967**, *38*, 37–42.
(22) Arora, A. K.; Yagi, T.; Miyajima, N.; Mary, T. A. *J. Appl. Phys.* **2005**, *97*, 013508.
(23) Hammersley, J. *Fit2d User Manual*; ESRF: Grenoble, France. 1996.
(24) Izumi, F.; Momma, K. *Solid State Phenom.* **2007**, *130*, 15–20.
(25) Koo, H. J.; Xiang, H; Lee, C.; Whangbo, M. H. *Inorg. Chem.* **2009**, *48*, 9051–9053.
(26) Yamada, H.; Ueda, Y. *J. Phys. Soc. Jpn.* **1999**, *68*, 2735–2740.
(27) Rogers, D. B.; Shannon, R. D.; Prewitt, C. T.; Gillson, J. L. *Inorg. Chem.* **1971**, *10*, 723–727.
(28) Derzsi, M. *Phys. Rev. B* **2009**, *79*, 205105.
(29) Birch, F. *J. Appl. Phys.* **1938**, *9*, 279–288.
(30) Errandonea, D.; Pellicer-Porres, J.; Manjón, F. J.; Segura, A.; Ferrer-Roca, C.; Kumar, R. S.; Tschauner, O.; Rodríguez-Hernández, P.; López-Solano, J.; Radescu, S.; Mujica, A.; Muñoz, A.; Aquilanti, G. *Phys. Rev. B* **2005**, *72*, 174106.
(31) Errandonea, D.; Kumar, R. S.; Ma, X; Tu, C. *J. Solid State Chem. B* **2008**, *181*, 355–364.
(32) Fischer, M.; Bonello, B.; Itié, J. P.; Polian, A.; Dartyge, E.; Fontaine, A.; Tolentino, H. *Phys. Rev. B* **1990**, *42*, 8494–8498.
(33) Chang, K. J.; Cohen, M. L. *Phys. Rev. B* **1984**, *30*, 4774–4781.
(34) Alfè, D.; Alfredsson, M.; Brodholt, J.; Gillan, M. J.; Towler, M. D.; Needs, R. J. *Phys. Rev. B* **2005**, *72*, 014114.
(35) Jeanloz, R.; Ahrens, T. J.; Mao, H. K.; Bell, P. M. *Science* **1979**, *206*, 829–830.
(36) Grzybwski, T. A.; Ruoff, A. L. *Phys. Rev. B* **1983**, *27*, 6502–6503.
(37) Narayana, C.; Nesamony, V. J.; Ruoff, A. L. *Phys. Rev. B* **1997**, *56*, 14338–14343.
(38) Sato, Y.; Jeanloz, R. *J. Geophys. Res. B* **1981**, *86*, 11773–11778.
(39) Sato, M.; Abo, J.; Jin, T.; Ohta, M. *J. Alloys Compd.* **1993**, *192*, 81–83.
(40) Kojima, K. M.; Fudamoto, Y.; Larkin, M.; Luke, G. M.; Merrin, J.; Nachumi, B; Uemura, Y. J.; Motoyama, N.; Eisaki, H.; Uchida, S.; Yamada, K.; Endoh, Y.; Hosoya, S.; Sternlieb, B. J.; Shirane, G. *Phys. Rev. Lett.* **1997**, *78*, 1787–1790.
(41) Wong-Ng, W. K.; Davis, K. L.; Roth, R. S. *J. Am. Ceram. Soc.* **1988**, *71*, C64–C67.
(42) Nagata, Y.; Taniguchi, T.; Tanaka, G.; Satho, M.; Samata, H. *J. Alloys Compd.* **2002**, *346*, 50–56.
(43) Rieck, H.; Hoppe, R. *Z. Anorg. Allg. Chem.* **1973**, *400*, 311–320.
(44) Dagotto, E.; Riera, J.; Scalapino, D. *Phys. Rev. B* **1992**, *45*, 5744–5747.
(45) Nagata, T.; Uehara, M.; Goto, J.; Akimitsu, J.; Motoyama, N.; Eisaki, H.; Uchida, S.; Takahashi, H.; Nakanishi, T.; Môri, N. *Phys. Rev. Lett.* **1998**, *81*, 1090–1093.